Colossal Shear-Strength Enhancement of Low-Density Cubic BC_2N by Nanoindentation

Zicheng Pan,[1] Hong Sun,[1,2,*,†] and Changfeng Chen[2,*,‡]

[1]*Department of Physics, Shanghai Jiao Tong University, Shanghai 200030, China*

[2]*Department of Physics and High Pressure Science and Engineering Center, University of Nevada, Las Vegas, Nevada 89154, USA*

(Received 11 September 2006; published 28 March 2007; corrected 29 March 2007)

Recently synthesized low-density cubic BC_2N exhibits surprisingly high shear strength inferred by nanoindentation in stark contrast to its relatively low elastic moduli. We show by first-principles calculation that this intriguing phenomenon can be ascribed to a novel structural hardening mechanism due to the compressive stress beneath the indenter. It significantly strengthens the weak bonds connecting the shear planes, yielding a colossal enhancement in shear strength. The resulting biaxial stress state produces atomistic fracture modes qualitatively different from those under pure shear stress. These results provide the first consistent explanation for a variety of experiments on the low-density cubic BC_2N phase across a large range of strain.

DOI: 10.1103/PhysRevLett.98.135505 PACS numbers: 62.20.−x, 81.40.Jj

For decades, engineers have relied on elastic and plastic models to describe and interpret the mechanical indentation process that measures material strength and hardness. Recent advances in nanometer-scale measurements and analysis have led to the discovery of a rich variety of new phenomena that go beyond the scope of these standard mechanical descriptions. Examples include indentation induced local phase transformation [1–3], bond switching [4], and dissipative kink band formation [5]. They all involve microscopic bond transformations that are not explicitly considered in macroscopic models. These results highlight the greatly increased need to examine the material response to nanoindentation at the atomistic level. Here we report on a first-principles study of a dramatic strength enhancement by nanoindentation on recently synthesized low-density cubic BC_2N (c-BC_2N) [6]. We examine the stark contrast between its relatively low elastic moduli, which imply low strength, and its high shear strength second only to that of diamond inferred by nanoindentation. We show that this dichotomy can be ascribed to a novel bond strengthening mechanism. The normal stress beneath the indenter plays a key role: it induces the rebonding of the weak bonds connecting the shear planes, yielding significant bond hardening and an unprecedented colossal enhancement of nearly sixfold increase in shear strength. The elucidation of the underlying atomistic mechanism enriches the fundamental understanding of nanomechanics.

The BC_2N has attracted considerable interest for its exceptional hardness exceeding that of cubic BN (c-BN) and its thermal stability superior to that of diamond [6–8]. However, a full understanding of its properties has been hindered by a lack of consistent description of its different (high- and low-density) phases. Most notable is the interpretation of the nanoindentation result of the low-density phase [6] that has a reported hardness of 76 GPa in between those of diamond (115 GPa) and c-BN (62 GPa) despite its fairly low-bulk modulus that is only 60% and 70% of the values for diamond and c-BN, respectively. A structural model proposed [9,10] for the high-density phases [7,8] was recently adopted by hardness calculations [11,12] on the low-density phase [6]; but it is clearly inconsistent with experiments. First, the x-ray diffraction measurement of the low-density phase [6] indicates a lattice constant that is considerably (1.5%) larger and a bulk modulus significantly (30%) lower than predicted by the high-density structural model [9]. In addition, a Brillouin scattering experiment on the same sample [13] detected low sound velocities that indicate the existence of weak bonds incompatible with the strong covalent bonding in the high-density model [10]. Meanwhile, first-principles total-energy and dynamic phonon calculations have identified a low-density structure (BC_2N-5 in Ref. [9,10]) whose lattice constants, elastic moduli, and sound velocities are in excellent agreement with the experimental data [6,13]. Its key structural feature is the weak N-N bonds connecting the {111} planes that cause the observed volume expansion from the ideal mixing value, the modest bulk modulus and the low sound velocity. However, it predicts low shear strength for this structure. The contrast with the high shear strength under nanoindentation presents a challenge to the understanding of the underlying nanomechanics.

Nanoindentation produces significant shear deformation beneath the indenter. The limit of the structural stability of the specimen is closely related to its maximum shear strength [14], which precedes the initiation of cracks and dislocations that lead to plastic deformation [15,16]. Empirical engineering models employ simple scaling functions for stress-strain relations in structural mechanics and in the design of strong solids [17,18]. Recent advances [15,16,19–22] have made it possible to calculate directly the ideal strength, i.e., the stress at which a perfect crystal becomes mechanically unstable, which sets an upper bound for the strength. These calculations also provide atomistic deformation modes and accurate stress-strain relations. The stress beneath the indenter contains a pure shear component and a normal compressive stress component that can reach tens or even hundreds of gigapascals

(GPa) [2,23,24]. The normal stress component is often not considered in ideal shear-strength calculations [19–22]. This may work well in cases where the normal stress is not very large, especially for superhard materials with high symmetry, such as diamond and c-BN [25]. However, very large normal stresses present beneath the indenter are expected to have significant effects, particularly on materials with anisotropic bonding weaknesses such as the low-density c-BC_2N. In the present work, we carry out ideal shear-strength calculations for the low-density c-BC_2N structure that explicitly include a normal stress component during the entire shear deformation process. The total-energy calculations were carried out using the local-density-approximation (LDA) pseudopotential scheme with a plane-wave basis set [26–28]. The norm-conserving Troullier-Martins pseudopotentials [29] were used with cutoff radii of 1.3, 1.3, 1.5 a.u. for N, C, and B, respectively. The exchange-correlation functional of Ceperley and Alder [27] as parametrized by Perdew and Zunger [30] was used. The total energy of the structures was minimized by relaxing the structural parameters using a quasi-Newton method [31]. The total-energy and stress calculations used an eight-atom zinc-blende-structured unit cell, an $8 \times 8 \times 8$ Monkhorst-Pack [32] k-point grid, and an 80 Ry energy cutoff. This method has been widely used in the study of crystalline solids and typically produces lattice constants within 1% and bulk and shear moduli within a few percent compared to experimental data. Our calculations conform to these standards. Moreover, the error in the calculated stresses due to the energy cutoff and k-point grid was less than 0.1 GPa based on convergence tests. The quasistatic ideal shear strength and relaxed loading path in easy slip planes were determined using a method described previously [19,20]. The lattice vectors were incrementally deformed in the direction of the applied strain. At each step, the applied strain in the easy slip plane is fixed which determines the calculated shear stress, while the other five independent components of the strain tensors and all the atoms inside the unit cell were simultaneously relaxed until (i) the stress normal to the easy slip plane reached a specified value, (ii) all the other residual components of the Hellmann-Feynman stress tensor orthogonal to the applied strain are less than 0.1 GPa, and (iii) the force on each atom becomes negligible. The shape of the unit cell is determined by this constrained atomic relaxation without any imposed boundary conditions.

To describe the biaxial stress under the indenter, we decompose the contact force between the indenter face and the specimen into two components: F_x parallel to the specimen surface and F_z perpendicular to the surface. They project onto the same contact area and produce a pure shear stress component $\sigma_{xz} = F_x/A_z$ and a normal compressive stress component $\sigma_{zz} = F_z/A_z$, where A_z is the projected area under the indenter. They are related by $\sigma_{zz}/\sigma_{xz} = \tan\Psi$, where Ψ is the centerline-to-face angle of the indenter. Since the Vickers, Knoop, and Berkovich indenters used in the hardness measurements [6] all have similarly large centerline-to-face angles, we use the Vickers indenter value of $\Psi = 68°$ in our calculations. The variation of a few degrees of the other indenters is not expected to change the conclusions.

The calculated stress-strain relations in the easy slip (111) plane along the weakest $[11\bar{2}]$ direction under the pure and biaxial shear stress are shown in Fig. 1 together with the corresponding bond length variations and several key structural snapshots. Under the pure shear stress, the weak bonding between the {111} shear planes easily soften, yielding a ideal shear strength of 11.7 GPa at the critical shear strain of 0.085 that is far too low to explain the experimental hardness result (76 GPa) [6]. This is consistent with the low density and low elastic moduli observed in the experiments [6,13] and previous calculations [9,10]. However, under the biaxial stress the normal stress σ_{zz} compresses the soft [111] N-N bonds, causing significant structural hardening as evidenced by the steeper rise of the stress-strain curve [Fig. 1(a)]. At the shear strain of 0.065, the [111] N-N bonds fully rebond, leading to a strained structure with all strong covalent bonds [Fig. 1(b) and 1(c)]. It results in a sharp jump in the shear strength from 18.2 GPa right before the rebonding (at S_1) to 33.6 GPa afterwards (at S_2). The rebonded structure produces a strong and enduring elastic response to the applied shear strain, yielding a peak (ideal) shear strength of 66.8 GPa at the critical shear strain of 0.220. It represents a colossal enhancement of nearly sixfold increase (from 11.7 GPa to 66.8 GPa) in shear strength compared to that under pure shear stress. This level of shear-strength enhancement by the normal compression is unprecedented in covalent solids. The resulting stress-strain curve [see Fig. 1(a)] splits into two parts, reflecting the drastically different structural characteristics before and after the rebonding of the [111] N-N bonds. It cannot be fit by a simple (e.g., sinusoidal) scaling function as commonly practiced in engineering models; instead, it must be described at the atomistic level. At larger shear strains, the [111] bonds that soften and break under the pure shear stress remain strong under the normal compression while the $[11\bar{1}]$ bonds in the {111} shear plane soften. The local fracture occurs as the $[11\bar{1}]$ N-C bonds break around the shear strain of 0.240 [Fig. 1(b) and 1(c)]. We further examined the structural stability under the normal stress component at the peak shear stress (at S_3). The calculated $\sigma_{zz} - \Delta\epsilon_{zz}$ curve [Fig. 1(a), inset] shows a strong positive response (increase) in σ_{zz} to increasing normal compressive strain $\Delta\epsilon_{zz}$. It clearly indicates the stability of the structure under σ_{zz} up to the peak shear stress. This demonstrates that the mechanism of the structural instability of the low-density c-BC_2N under the biaxial stress is the $(111)[11\bar{2}]$ shear softening with the breaking of the $[11\bar{1}]$ N-C bonds instead of the [111] N-N bonds as under pure shear stress.

Recent hardness calculations [11,12] adopted a high-density structural model [9] but compared the calculated hardness with that of the low-density c-BC_2N [6] despite

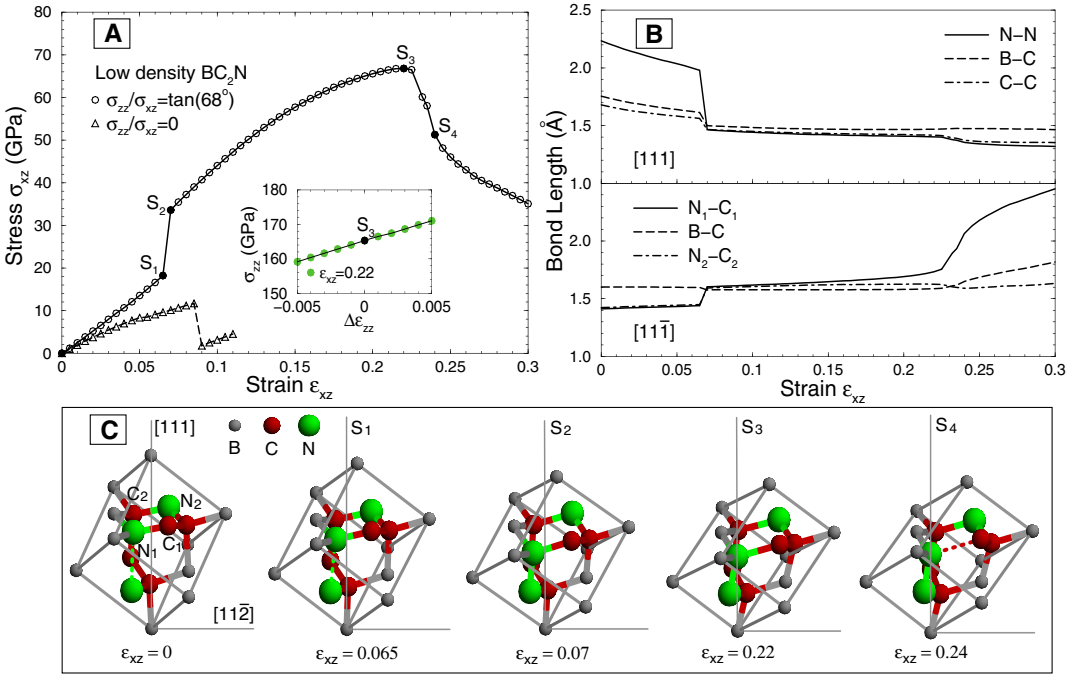

FIG. 1 (color online). (a) The calculated stress-strain relations of the low-density c-BC_2N under the (111)[11$\bar{2}$] pure shear ($\sigma_{zz}/\sigma_{xz} = 0$) and biaxial ($\sigma_{zz}/\sigma_{xz} = \tan 68°$) stress. The inset shows the response of the normal compressive stress (σ_{zz}) to the variation of the normal compressive strain ($\Delta\epsilon_{zz}$) at the (fixed) critical shear strain $\epsilon_{xz} = 0.22$ (S_3). (b) The length variation of the [111] bonds that connect the {111} shear planes and the [11$\bar{1}$] bonds that are in the {111} shear planes under the biaxial stress. (c) The snapshots of the calculated structural unit cell at equilibrium ($\epsilon_{xz} = 0$) and at four key points on the stress-strain curve under the biaxial stress shown in (a). The dashed lines indicate the weak (broken) bonds.

that the calculated bulk modulus [9] and sound velocities [10] for this high-density structure are inconsistent with the x-ray and Brillouin scattering experiments [6,13]. Here we start from the correct low-density equilibrium structure that is in full agreement with the experimental data [9,10] and demonstrate a stress-induced structural hardening that provides a consistent explanation for its structural properties at equilibrium and the high shear strength under nanoindentation.

The most distinguished property of the low-density c-BC_2N is that it is stronger under indentation compared to c-BN that is the second (only to diamond) hardest material known. It is therefore important to examine c-BN under the same loading conditions. The calculated results are presented in Fig. 2. Under pure shear stress, the ideal shear strength of c-BN is 70.4 GPa, which is 6 times that (11.7 GPa) of the low-density c-BC_2N. Under the loading condition $\sigma_{zz}/\sigma_{xz} = \tan 68°$, the effect of σ_{zz} is initially very small up to $\epsilon_{xz} = 0.20$; beyond that there is an appreciable reduction in the shear strength. A close examination of the structural response to σ_{zz} shows that the primary deformation mode is the compressive softening of the [111] B-N bonds and beyond a critical strain $\epsilon_{xz} = 0.38$ near the peak shear stress [point S in Fig. 2(a); the structural snapshot is shown in Fig. 2(b)] the structure becomes unstable. At $\epsilon_{xz} = 0.395$ increasing compressive strain $\Delta\epsilon_{zz}$ generates a decisively negative response (decrease) in σ_{zz} [see the inset in Fig. 2(a)]. The interplay of the two stress components ends with the shear deformation giving way to the compressive failure mode when the [111] B-N bonds can no longer sustain the compressive stress and collapse before any shear induced bond breaking occurs. This atomistic mechanism for the structural instability of c-BN under the biaxial stress is qualitatively different from the shear failure mode under a pure shear stress [16,22]. The ideal shear strength of c-BN is reduced to 64.3 GPa, below the value (66.8 GPa) for the low-density c-BC_2N. Given the well-established positive correlation between the peak shear strength and hardness [18], these results provide a natural explanation for the high hardness of low-density c-BC_2N exceeding that of c-BN under nanoindentation [6].

In summary, our first-principles calculations show that the biaxial stress state beneath the indenter induces the reformation of the bonds connecting the shear planes, explaining why the low-density c-BC_2N can be elastically more compliant but still harder under indentation than c-BN. The results provide the first consistent explanation of its structural properties across a large range of strain and unveil the different fracture mechanisms under the biaxial stress in low-density c-BC_2N and c-BN: the (111)[11$\bar{2}$] shear softening with the breaking of the [11$\bar{1}$] N-C bonds in the former and the compressive collapse of the [111] B-N bonds in the latter. These atomistic fracture modes are

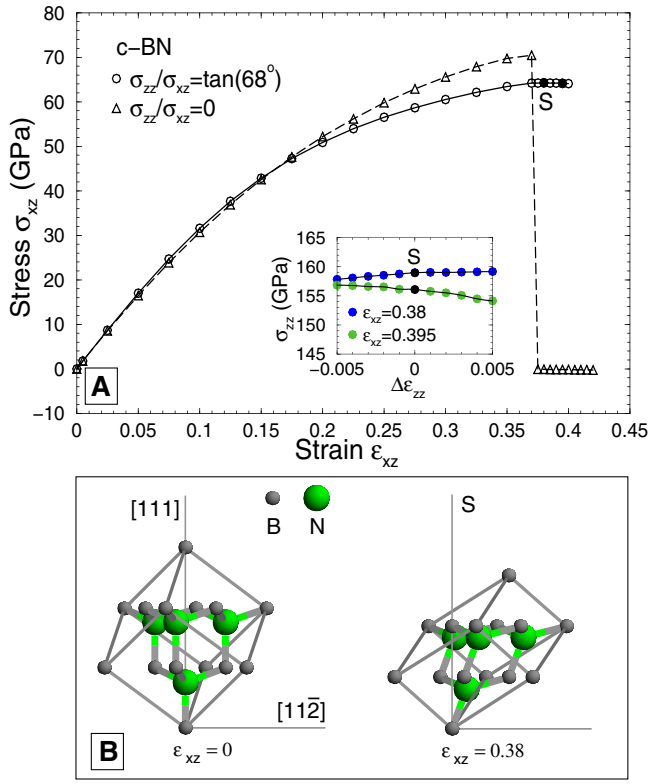

FIG. 2 (color online). (a) The calculated stress-strain relations of cubic boron nitride (c-BN) under the (111)[11$\bar{2}$] pure shear ($\sigma_{zz}/\sigma_{xz} = 0$) and biaxial ($\sigma_{zz}/\sigma_{xz} = \tan 68°$) stress. The inset shows the response of the normal compressive stress (σ_{zz}) to the variation of the normal compressive strain ($\Delta\epsilon_{zz}$) at two fixed shear strains ($\epsilon_{xz} = 0.38$ and 0.395) near the peak shear stress. (b) The snapshots of the calculated structural unit cell at equilibrium ($\epsilon_{xz} = 0$) and at the critical shear strain $\epsilon_{xz} = 0.38$ under $\sigma_{zz}/\sigma_{xz} = \tan 68°$ right before the collapse of the [111] B-N bonds.

qualitatively different from their counterparts under pure shear stress, which have broad implications for understanding the structural properties. The computational approach and the atomistic description of the structural deformation under a biaxial stress can be extended to examining and interpreting the results of other materials under nanoindentation that is increasingly applied beyond its original scope of hardness testing and becoming a versatile tool for material characterization [1–5]. Several aspects not considered here, such as the nonuniform pressure distribution, nonlinear stress-strain behavior, and the complex stress state beyond the biaxial description beneath the indenter, may improve quantitative comparison with experiment. However, the role of the normal compression in the reformation of the [111] N-N bonds and the resulting qualitative change in the atomistic fracture modes should remain the key to understanding the observed colossal shear-strength enhancement in the low-density c-BC_2N.

This work was supported by the DOE Grant No. DE-FC52-06NA26274. H. S. was also supported by the National Natural Science Foundation of China Grants No. 10574089 and No. 50532020 and the High Performance Computing Center at Shanghai Jiao Tong University.

*To whom correspondence should be addressed.
†Email address: hsun@sjtu.edu.cn
‡Email address: chen@physics.unlv.edu

[1] G. S. Smith, E. B. Tadmor, and E. Kaxiras, Phys. Rev. Lett. **84**, 1260 (2000).
[2] Y. G. Gogotsi, A. Kailer, and K. G. Nickel, Nature (London) **401**, 663 (1999).
[3] J. Jang *et al.*, Acta Mater. **53**, 1759 (2005).
[4] W. Guo *et al.*, Phys. Rev. Lett. **93**, 245502 (2004).
[5] M. W. Barsoum *et al.*, Phys. Rev. Lett. **92**, 255508 (2004).
[6] V. L. Solozhenko *et al.*, Appl. Phys. Lett. **78**, 1385 (2001).
[7] E. Knittle *et al.*, Phys. Rev. B **51**, 12 149 (1995).
[8] Y. Zhao *et al.*, J. Mater. Res. **17**, 3139 (2002).
[9] H. Sun *et al.*, Phys. Rev. B **64**, 094108 (2001).
[10] Z. C. Pan, H. Sun, and C. F. Chen, Phys. Rev. B **70**, 174115 (2004).
[11] F. Gao *et al.*, Phys. Rev. Lett. **91**, 015502 (2003).
[12] A. Simunek and J. Vackar, Phys. Rev. Lett. **96**, 085501 (2006).
[13] S. N. Tkachev *et al.*, Phys. Rev. B **68**, 052104 (2003).
[14] A. Gouldstone *et al.*, Acta Mater. **48**, 2277 (2000).
[15] S. Ogata, J. Li, and S. Yip, Science **298**, 807 (2002).
[16] S. Ogata *et al.*, Phys. Rev. B **70**, 104104 (2004).
[17] D. M. Teter, Mater. Res. Bull. **23**, 22 (1998).
[18] V. V. Brazhkin, A. G. Lyapin, and R. J. Hemley, Philos. Mag. A **82**, 231 (2002).
[19] D. Roundy *et al.*, Philos. Mag. A **81**, 1725 (2001).
[20] D. Roundy *et al.*, Phys. Rev. Lett. **82**, 2713 (1999).
[21] D. M. Clatterbuck *et al.*, Phys. Rev. Lett. **91**, 135501 (2003).
[22] Y. Zhang, H. Sun, and C. F. Chen, Phys. Rev. Lett. **93**, 195504 (2004); **94**, 145505 (2005).
[23] K. J. Van Vliet *et al.*, Phys. Rev. B **67**, 104105 (2003).
[24] T. Zhu *et al.*, J. Mech. Phys. Solids **52**, 691 (2004).
[25] For results on diamond, see, H. Chacham and L. Kleinman, Phys. Rev. Lett. **85**, 4904 (2000). We performed calculations on c-BN under the same loading conditions with a fairly large normal compression of 50 GPa and obtained a very small (1.3%) enhancement in the ideal shear strength over that without the normal compression.
[26] J. Ihm, A. Zunger, and M. L. Cohen, J. Phys. C **12**, 4409 (1979).
[27] D. M. Ceperley and B. J. Alder, Phys. Rev. Lett. **45**, 566 (1980).
[28] M. L. Cohen, Phys. Scr. **T1**, 5 (1982).
[29] N. Troullier and J. L. Martins, Phys. Rev. B **43**, 1993 (1991).
[30] J. P. Perdew and A. Zunger, Phys. Rev. B **23**, 5048 (1981).
[31] B. G. Pfrommer *et al.*, J. Comput. Phys. **131**, 233 (1997).
[32] H. J. Monkhorst and J. D. Pack, Phys. Rev. B **13**, 5188 (1976).